



The properties of iron under core conditions from first principles calculations

L. Vočadlo^a, D. Alfè^{a,b}, M.J. Gillan^b, G. David Price^{a,*}

^a *Research School of Earth Sciences, Birkbeck and University College London, Gower Street, London WC1E 6BT, UK*

^b *Department of Physics and Astronomy, University College London, Gower Street, London WC1E 6BT, UK*

Accepted 11 August 2003

Abstract

The Earth's core is largely composed of iron (Fe). The phase relations and physical properties of both solid and liquid Fe are therefore of great geophysical importance. As a result, over the past 50 years the properties of Fe have been extensively studied experimentally. However, achieving the extreme pressures (up to 360 GPa) and temperatures (~ 6000 K) found in the core provide a major experimental challenge, and it is not surprising that there are still considerable discrepancies in the results obtained by using different experimental techniques. In the past 15 years quantum mechanical techniques have been applied to predict the properties of Fe. Here we review the progress that has been made in the use of first principles methods in the study of Fe, and focus upon (i) the structure of Fe under core conditions, (ii) the high P melting behaviour of Fe, (iii) the thermodynamic properties of hexagonal close-packed (hcp) Fe, and (iv) the rheological and thermodynamic properties of high P liquid Fe.

© 2003 Elsevier B.V. All rights reserved.

Keywords: Earth's core; Molecular dynamics; Ab initio methods; Iron

1. Introduction

The fact that the core is largely composed of Fe was firmly established as a result of Birch's (1952) analysis of mass-density/sound-wave velocity systematics. Today we believe that the outer core is about 6–10% less dense than pure liquid Fe, while the solid inner-core is a few percent less dense than crystalline Fe (e.g. Poirier, 1994a). From cosmochemical and other considerations, it has been suggested (e.g. Poirier, 1994b; Allègre et al., 1995; McDonough and Sun, 1995) that the alloying elements in the core might include S, O, Si, H and C. It is also probable that the core contains minor amounts of other elements, such as Ni and K.

The exact temperature profile of the core is still controversial (e.g. Alfè et al., 2002a), but it is generally held that the inner-core is crystallising from the outer core as the Earth slowly cools, and that core temperatures are in the range 4000–7000 K, while the pressure at the centre of the Earth is ~ 360 GPa.

Before a full understanding of the chemically complex core is reached, it is necessary to understand the properties and behaviour at high pressure (P) and temperatures (T) of its primary constituent, namely metallic Fe. Experimental techniques have evolved rapidly in the past years, and today using diamond anvil cells (DAC) or shock experiments the study of minerals at pressures up to ~ 200 GPa and temperatures of a few thousand Kelvin is possible. These studies, however, are still far from routine, and results from different groups are often in conflict (see for example reviews

* Corresponding author.

E-mail address: d.price@ucl.ac.uk (G.D. Price).

by Poirier, 1994b; Shen and Heinze, 1998; Stixrude and Brown, 1998; Boehler, 2000). As a result, therefore, in order to complement these existing experimental studies and to extend the range of pressure and temperature over which we can model the Earth, computational mineral physics has, in the past decade, become an established and growing discipline.

Within computational mineral physics a variety of atomistic simulation methods (developed originally in the fields of solid state physics and theoretical chemistry) are used. These techniques can be divided approximately into those that use some form of interatomic potential model to describe the energy of the interaction of atoms in a mineral as a function of atomic separation and geometry, and those that involve the approximate solution of Schrödinger equation to calculate the energy of the mineral species by quantum mechanical techniques. For the Earth sciences, the accurate description of the behaviour of minerals as a function of temperature is particularly important, and computational mineral physics usually uses either lattice dynamics or molecular dynamics (MD) methods to achieve this important step. The relatively recent application of all of these advanced condensed matter physics methods to geophysics has only been made possible by the very rapid advances in the power and speed of computer processing. Techniques, which in the past were limited to the study of structurally simple compounds, with small unit cells, can today be applied to describe the behaviour of complex, low symmetry structures (which epitomise most minerals) and liquids.

In this paper, we will focus on recent studies of Fe, which have been aimed at predicting its geophysical properties and behaviour under core conditions. Although interatomic potentials have been used to study Fe (e.g. Matsui and Anderson, 1997), many of its properties are very dependent upon a precise description of its metallic nature and can only be modelled accurately by quantum mechanical methods. Thus, below we outline the essential *ab initio* techniques used in the most recent studies of Fe (see also Stixrude et al., 1998). We then present a discussion of the structure of the stable phase of Fe at core pressures and temperatures, its melting behaviour at core pressures, and *ab initio* estimates of the high *P/T* physical and thermodynamic properties of both liquid and crystalline iron.

2. Quantum mechanical simulations

Ab initio simulations are based on the description of the electrons within a system in terms of a quantum mechanical wave function, ψ , the energy and dynamics of which is governed by the general Schrödinger equation for a single electron:

$$i\hbar \frac{\partial \psi}{\partial t} = -\frac{\hbar^2}{2m} \nabla^2 \psi + V(r)\psi \quad (1)$$

where $V(r)$ is the potential energy of the system and the other terms take their usual meaning. In minerals, however, it is necessary to take into account all of the electrons within the crystal, so the energy, E , of a many electron wave function, Ψ , is required:

$$E\Psi(r_1, r_2, \dots, r_N) = \left(\sum -\frac{\hbar^2}{2m} \nabla^2 + V_{\text{ion}} + V_{\text{e-e}} \right) \Psi(r_1, r_2, \dots, r_N) \quad (2)$$

In a confined system, the electrons experience interactions between the nuclei and each other. This interaction may be expressed in terms of an ionic contribution and a Coulombic contribution (the second and third terms within the brackets). Energy minimisation techniques may be applied in order to obtain the equilibrium structure for the system under consideration.

Unfortunately, the complexity of the wave function, Ψ , for an N electron system scales as M^N , where M is the number of degrees of freedom for a single electron wave function, Ψ . This type of problem cannot readily be solved for large systems due to computational limitations, and therefore the exact solution to the problem for large systems is intractable. However, there are a number of approximations that may be made to simplify the calculation, whereby good predictions of the structural and electronic properties of materials can be obtained by solving self-consistently the one-electron Schrödinger equation for the system, and then summing these individual contributions over all the electrons in the system (for more detailed reviews see Gillan (1997) and Stixrude et al. (1998)). Such approximation techniques include the Hartree Fock approximation (HFA) and density functional theory (DFT), which differ in their description of the electron–electron interactions. In both cases the

average electrostatic field surrounding each electron is treated similarly, reducing the many body Hamiltonian in the Schrödinger equation for a non-spin-polarised system (i.e. ignoring any spin alignment and resulting magnetic effects) to that for one electron surrounded by an effective potential associated with the interactions of the surrounding crystal. However, the difference between the two methods arises in the treatment of the contribution to the potential associated with the fact that the electron is not in an average field, the correlation, and also in the treatment of the electronic spin governed by Pauli's exclusion principle, the exchange. In the HFA the exchange interactions are treated exactly, but the correlation is not included; in modern geophysical investigations of silicates and iron phases, DFT is increasingly favoured, where the exchange and correlation are both included but, in current approximations, only in an average way (see Stixrude et al. (1998) for more details).

Density functional theory, originally developed by Hohenberg and Kohn (1964) and Kohn and Sham (1965), describes the exact ground state properties of a system in terms of a unique functional of charge density alone, i.e. $E = E(\rho)$. The Hohenberg–Kohn theorem says that the ground state density uniquely determines the potential (and so all equilibrium physical properties of the system). Using the variational principle it is easy to show that the ground state density minimises the total-energy. So by looking for the minimum of the total-energy, we find the ground state density. In DFT, the electronic energy may be written:

$$E_{\text{electronic}} = \int V_{\text{ion}}(r)\rho(r) d^3r + E_{\text{electrostatic}} + E_{\text{xc}}[\rho] \quad (3)$$

Therefore, by varying the electron density of the system through a search of single particle density space until the minimum energy configuration is found, an exact ground state energy is achieved, and that electron density is the exact ground state energy for the system; all other ground state properties are all functions of this ground state electron density. However, the exact form of the functional $E_{\text{xc}}[\rho]$ is not known, and is approximated by a local function of the density. This local density approximation (LDA) defines the exchange-correlation potential as a function of electron density at a given co-ordinate position (Kohn and Sham, 1965). Sometimes it is a better approximation

to use the generalised gradient approximation (GGA) (e.g. Wang and Perdew, 1991), which has a similar form for the exchange-correlation potential, but has it as a function of both the local electron density and the magnitude of its gradient. For simulations of Fe, the use of GGA is very important, as the use of LDA leads to the prediction of the wrong ground state (Stixrude et al., 1998).

The correct description of magnetic effects can be vital in determining the accuracy of the simulation of the stability and physical properties of some phases. Thus for example, the body centred cubic (bcc) polymorph of Fe is only stable at ambient conditions because of its strongly developed ferromagnetism (e.g. see Stixrude and Brown, 1998). Steinle-Neumann et al. (1999) have shown how the calculated equation of state of hcp Fe is dependent upon the correct inclusion of local spin polarisation, and more recently Mukherjee and Cohen (2002) have shown the importance of using fully unconstrained non-collinear magnetism to describe the properties of magnetically more complex phases. Fortunately, for Fe under core conditions, Söderlind et al. (1996) have shown that the high pressures destroy most of the magnetic states that Fe polymorphs exhibit at lower pressure, but nevertheless, studies of high P/T behaviour of Fe must recognise the potential importance of that magnetic interactions may have on the physical and thermodynamic properties of the Fe polymorphs.

In any implementation of DFT the description of electron spin states naturally requires a way of efficiently describing the electron wave functions, $\Psi_i(\mathbf{r})$. One approach is to describe $\Psi_i(\mathbf{r})$ as a sum of basis-sets made up of atomic wave functions, $\varphi_\alpha(\mathbf{r})$:

$$\Psi_i(\mathbf{r}) = \sum_{\alpha} c_{i\alpha} \varphi_{\alpha}(\mathbf{r}) \quad (4)$$

The other approach is to use basis functions that describe the itinerant nature of electrons, and which are based on the wave function of a free electron, $\exp(i\mathbf{k}\cdot\mathbf{r})$, where \mathbf{k} is the wave vector of the de Broglie wave. Thus $\Psi_i(\mathbf{r})$ can now be expressed as a sum of possible plane-wave basis functions:

$$\Psi_i(\mathbf{r}) = \sum_{\mathbf{k}} c_{i\mathbf{k}} \exp(i\mathbf{k}\cdot\mathbf{r}) \quad (5)$$

In fact, both approaches are valid, but in practice for the large numbers of atoms usually involved in

condensed matter simulations, the plane-wave method has to date been much more successful. This might appear at first sight to be surprising, because the electrons in condensed matter are clearly not like free particles, as in most atoms there are tightly bound core electrons confined around the nucleus. To describe these core electrons requires the inclusion of a very large number of plane-waves. There are techniques, such as the linearized augmented plane-wave (LAPW) method, that do this and provide very accurate descriptions of the potential and charge density within the entire crystal (for more details see for example [Stixrude et al., 1998](#)). The number of electrons (and hence atoms) to which this approach can be applied is limited, however, by current computing capacity, and it cannot be used efficiently for large or complex systems.

An alternative to the ‘all electron technique’ is to use electronic wave functions that are expanded in a plane-wave basis-set, with the electron–ion interactions described by means of pseudopotentials. A pseudopotential is a modified form of the true potential experienced by the electrons ([Heine, 1970](#); [Cohen and Heine, 1970](#); [Heine and Weaire, 1970](#)). When they are near the nucleus, the electrons feel a strong attractive potential and this gives them a high kinetic energy. But this means that their de Broglie wavelength is very small, and their wave vector is very large. As mentioned above, because of this, a plane-wave basis would have to contain so many wave vectors that the calculations would become very demanding. A remarkable way of eliminating this problem and broadening the range of systems that can be studied was developed by Heine, Cohen and others, who showed that it is possible to represent the interaction of the valence electrons with the atomic cores by a weak effective ‘pseudopotential’ and still end up with a correct description of the electron states and the energy of the system. In this way of doing things, the core electrons are assumed to be in exactly the same states that they occupy in the isolated atom, which is usually valid. There are several ways of constructing pseudopotentials, and it is essential to show that they correctly describe the system under study, but when this is done, it has been found that results obtained employing pseudopotentials are as reliable as those from all electron calculations.

More recently the projector augmented wave (PAW) method has increasingly been used (e.g. [Kresse and](#)

[Joubert, 1999](#)). The PAW approach is an all electron method in the sense that it works with the true Kohn–Sham orbitals, rather than orbitals that have been ‘pseudised’ in the core regions, and it has the same level of rigour as other all electron methods such as FLAPW. At the same time it is very closely related to the ultra soft pseudopotential technique ([Vanderbilt, 1990](#)), and reduces to this if certain well-defined approximations are used, as shown by [Kresse and Joubert \(1999\)](#). The PAW method has, therefore, the computational efficiency of the pseudopotential method, but without the minor drawback of the approximation involved in their formulation.

In conclusion, therefore, plane-waves have proved to be very successful for many reasons. The wave functions can be made as accurate as necessary by increasing the number of plane-waves, so that the method is systematically improvable. Plane-waves are simple so that the programming is easy, and it also turns out that the forces on the ions are straightforward to calculate, so that it is easy to move them. Finally, plane-waves are unbiased. The calculations are unaffected by the prejudices of the user—an important advantage for any method that is going to be widely used. As such using GGA within DFT combined with pseudopotentials or PAW methods provides an excellent technique with which to accurately explore most crystal structures (although it should be noted that DFT is not entirely free of limitations, some of which are discussed for example in [Stixrude et al. \(1998\)](#)). Below, we outline the application of these methods to the study of Fe. However to study Fe under core conditions, we need not only to explore the energetics of bonding, but we are also concerned with the effect of temperature on the system. This requires us to calculate the Gibbs free energy of the systems, which can be done either using lattice dynamic or molecular dynamic methods.

3. Lattice dynamics

Lattice dynamics is a semi-classical approach that uses the quasiharmonic approximation (QHA) to describe a cell in terms of independent quantised harmonic oscillators, the frequencies of which vary with cell volume, thus allowing for a description of thermal expansion (e.g. [Born and Huang, 1954](#)). The motions of the individual particles are treated

collectively as lattice vibrations or phonons, and the phonon frequencies, $\omega(q)$, are obtained by solving:

$$m\omega^2(q)e_i(q) = D(q)e_j(q) \quad (6)$$

where m is the mass of the atom, and the dynamical matrix, $D(q)$, is defined by:

$$D(q) = \sum_{ij} \left(\frac{\partial^2 U}{\partial u_i \partial u_j} \right) \exp(iq \cdot r_{ij}) \quad (7)$$

where r_{ij} is the interatomic separation, and u_i and u_j are the atomic displacements from their equilibrium position. For a unit cell containing N atoms, there are $3N$ eigenvalue solutions ($\omega^2(q)$) for a given wave vector q . There are also $3N$ sets of eigenvectors ($e_x(q)$, $e_y(q)$, $e_z(q)$) which describe the pattern of atomic displacements for each normal mode.

The vibrational frequencies of a lattice can be calculated ab initio, by standard methods such as the small-displacement method (e.g. Kresse et al., 1995). Having calculated the vibrational frequencies, a number of thermodynamic properties may be calculated using standard statistical mechanical relations, which are direct functions of these vibrational frequencies. Thus for example the Helmholtz free energy is given by:

$$F = k_B T \sum_i^M \left(\frac{x_i}{2} + \ln(1 - e^{-x_i}) \right) \quad (8)$$

where $x_i = \hbar\omega_i/k_B T$, and the sum is over all the $M = 3N$ normal modes. Modelling the effect of pressure is essential if one is to obtain accurate predictions of phenomena such as phase transformations and anisotropic compression. This problem is now routinely being solved using codes that allow constant stress, variable geometry cells in both static and dynamic simulations. In the case of lattice dynamics, the mechanical pressure is calculated from strain derivatives, whilst the thermal kinetic pressure is calculated from phonon frequencies (e.g. Parker and Price, 1989). The balance of these forces can be used to determine the variation of cell size as a function of pressure and temperature.

The quasi-harmonic approximation assumes that the lattice vibrational modes are independent. However at high temperatures, where vibrational amplitudes become large, phonon–phonon scattering becomes important, and the QHA breaks down. At ambient

pressure, the QHA is only valid for $T < \theta_D$, the Debye temperature, so since we are interested in the extreme conditions of the interior Earth, we would expect to have to modify this methodology to enable higher temperatures to be simulated (see e.g. Ball, 1989), alternatively we could use molecular dynamics techniques. Matsui et al. (1994) have shown, however, that the inherent anharmonicity associated with lattice dynamics decreases with increasing pressure, and the two techniques give very similar results for very high pressure and temperature simulations. It should be noted that another approach has been used by some workers (e.g. Stixrude et al., 1997) to calculate the effect of T on the properties of the high P phases of Fe. They use a mean-field approach known as the particle-in-cell (PIC) method. This method attempts to account for anharmonicity and is computationally efficient. A detailed comparison of the relative precision of the PIC method and molecular dynamic simulations of Fe have been presented by Alfè et al. (2001). Generally the molecular dynamics approach should be favoured as it involves far fewer approximations, but it is much more computationally intensive. We note, however, that the PIC method has the same level of complexity as the QHA, which treats harmonic vibrations exactly, but we have recently shown that the anharmonicity predicted by the PIC method has the *wrong* sign (Gannarelli et al., 2003), which weakens the case for preferring this approximation to that of the QHA.

4. Molecular dynamics

Molecular dynamics is routinely used for medium to high temperature simulations of minerals and in all simulations of liquids, where lattice dynamics is of course inapplicable. The method is essentially classical, and its details are presented in, for example, Allen and Tildesley (1987). The interactions between the atoms within the system have traditionally been described in terms of the interatomic potential models mentioned earlier, but instead of treating the atomic motions in terms of lattice vibrations, each ion is treated individually. As the system evolves, the required dynamic properties are calculated iteratively at the specified pressure and temperature. The ions are initially assigned positions and velocities within the simulation box; their co-ordinates are usually chosen

to be at the crystallographically determined sites, whilst their velocities are equilibrated such that they concur with the required system temperature, and such that both energy and momentum is conserved. In order to calculate subsequent positions and velocities, the forces acting on any individual ion are then calculated from the first derivative of the potential function, and the new position and velocity of each ion may be calculated at each time-step by solving Newton's equation of motion. Both the particle positions and the volume of the system, or simulation box, can be used as dynamical variables, as is described in detail in Parrinello and Rahman (1980). The kinetic energy, and therefore temperature, is obtained directly from the velocities of the individual particles. With this explicit particle motion, the anharmonicity is implicitly accounted for at high temperatures.

Because of advances in computer power, it is now possible to perform ab initio molecular dynamics (AIMD), with the forces calculated fully quantum mechanically (within the GGA and the pseudopotential or PAW approximations) instead of relying upon the use of interatomic potentials. The first pioneering work in AIMD was that of Car and Parrinello (1985), who proposed a unified scheme to calculate ab initio forces on the ions and keep the electrons close to the Born-Oppenheimer surface while the atoms move. We have used in the work summarised below an alternative approach, in which the dynamics are performed by explicitly minimising the electronic free energy functional at each time step. This minimisation is more expensive than a single Car-Parrinello step, but the cost of the step is compensated by the possibility of making longer time steps. The molecular dynamics simulations presented here have been performed using Vienna ab initio simulation package (VASP). In VASP the electronic ground state is calculated exactly (within a self-consistent threshold) at each MD step, using an efficient iterative matrix diagonalization scheme and the mixer scheme of Pulay (1980). We have also implemented a scheme to extrapolate the electronic charge density from one step to the next, with an efficiency improvement of about a factor of two (Alfè, 1999). Since we are interested in finite-temperature simulations, the electronic levels are occupied according to the Fermi statistics corresponding to the temperature of the simulation. This prescription also avoids problems with level crossing

during the self-consistent cycles. For more details of the VASP code see Kresse and Furthemüller (1996).

It is not possible to obtain free energies directly from MD techniques. These can, however, be obtained by 'thermodynamic integration', which yields the difference between the free energy (ΔF) of the ab initio system and that of a reference system. The basis of the technique (see for example de Wijs et al., 1998) is that ΔF is the work done on reversibly and isothermally switching from the reference total-energy function, U_{ref} , to the ab initio total-energy, U . This switching is done by passing through intermediate total-energy functions U_λ given by $U_\lambda = (1 - \lambda)U_{\text{ref}} + \lambda U$. It is a standard result that the work done is:

$$\Delta F = \int_0^1 d\lambda \langle U - U_{\text{ref}} \rangle_\lambda \quad (9)$$

where the thermal average $\langle U - U_{\text{ref}} \rangle_\lambda$ is evaluated for the system governed by U_λ . The practical feasibility of calculating ab initio free energies of liquids and anharmonic solids depends on finding a reference system for which F_{ref} is readily calculable and the difference ($U - U_{\text{ref}}$) is very small. However, we stress that the final result is independent on the choice of the reference system. In our studies of liquid Fe, the primary reference state chosen was an inverse power potential. The full technical details involved in our calculations are given in Alfè et al. (2002a,b,c). Below, we illustrate our use of all of these methods in the study of Fe at extreme pressure and temperature.

5. The structure of Fe under core conditions

Under ambient conditions, Fe adopts a body centred cubic (bcc) structure, that transforms with temperature to a face centred cubic (fcc) form, and with pressure transforms to a hexagonal close-packed (hcp) phase, ϵ -Fe. The high P/T phase diagram of pure iron itself however is still controversial (see Fig. 1 and also the discussion in Stixrude and Brown (1998)). Various diamond anvil cell based studies have been interpreted as showing that hcp Fe transforms at high temperatures to a phase which has variously been described as having a double hexagonal close-packed structure (dhcp) (Saxena et al., 1996) or an orthorhombically distorted hcp structure (Andrault et al., 1997). Furthermore, high pressure shock experiments have also been

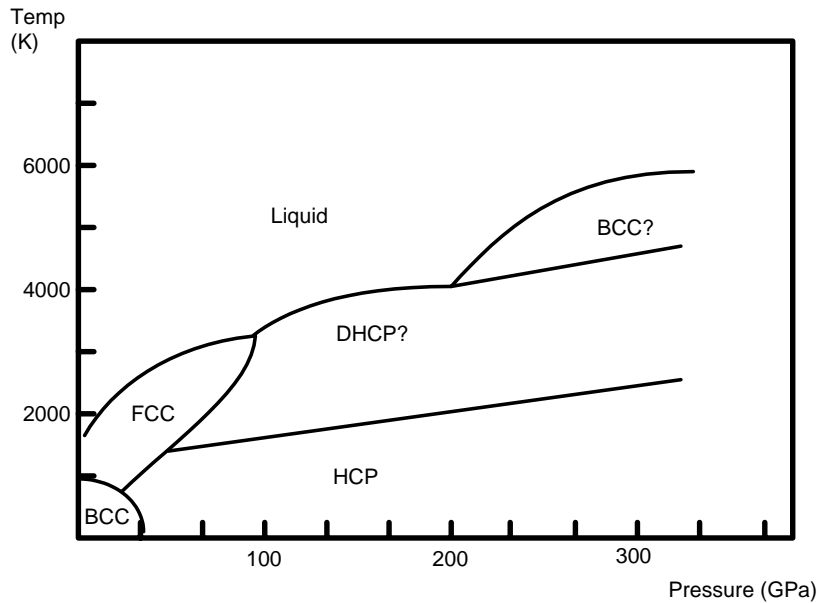


Fig. 1. A hypothetical phase diagram for Fe, incorporating all the experimentally suggested high P/T phase transformations. Our calculations suggest that the phase diagram is in fact much more simple than this, with hcp Fe being the only high P/T phase stable at core pressures.

interpreted as showing a high pressure solid–solid phase transformation (Brown and McQueen, 1986; Brown, 2001), which has been suggested could be due to the development of a bcc phase (Matsui and Anderson, 1997). Other experimentalists, however, have failed to detect such a post-hcp phase (e.g. Shen et al., 1998; Nguyen and Holmes, 1999), and have suggested that the previous observations were due either to minor impurities or to metastable strain-induced behaviour.

Further progress in interpreting the nature and evolution of the core would be severely hindered if the uncertainty concerning the crystal structure of the core's major chemical component remained unresolved. Such uncertainties can be resolved, however, using ab initio calculations, which we have shown provide an accurate means of calculating the thermoelastic properties of materials at high P and T (e.g. Vočadlo et al., 1999). Thermodynamic calculations on hcp Fe and fcc Fe at high P/T were reported by Wasserman et al. (1996) and by Stixrude et al. (1997). They used ab initio calculations to parameterise a tight-binding model; the thermal properties of this model were then obtained using the particle-in-a-cell method. The calculations that we performed (Vočadlo et al., 1999) to determine the high P/T structure of Fe, were the

first in which *fully* ab initio, non-parameterised methods were used, in conjunction with quasiharmonic lattice dynamics, to obtain free energies under core conditions of all the proposed candidate Fe structures.

Spin polarised simulations were initially performed on candidate phases (including a variety of distorted bcc and hcp structures and the dhcp phase) at pressures ranging from 325 to 360 GPa. These revealed, in agreement with Söderlind et al. (1996), that under these conditions only bcc Fe has a residual magnetic moment and all other phases have zero magnetic moments. It should be noted however, that the magnetic moment of bcc Fe disappears when simulations are performed at core pressures and an electronic temperature of >1000 K, indicating that even bcc Fe will have no magnetic stabilisation energy under core conditions. We found that at these pressures, both the bcc and the suggested orthorhombic polymorph of iron (Andrault et al., 1997) are mechanically unstable. The bcc phase can be continuously transformed to the fcc phase (confirming the findings of Stixrude and Cohen, 1995), while the orthorhombic phase spontaneously transforms to the hcp phase, when allowed to relax to a state of isotropic stress. In contrast, hcp, dhcp and fcc Fe remain mechanically stable at core pressures,

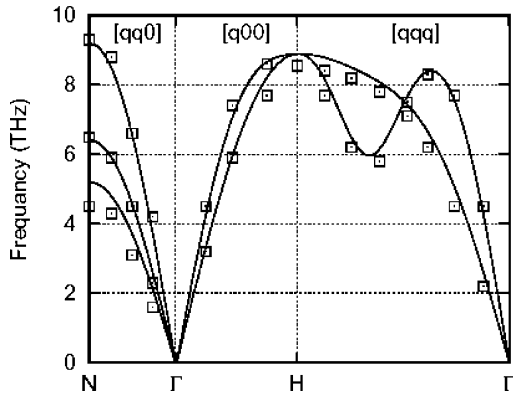


Fig. 2. The phonon-dispersion curves along a $\Gamma\text{H}\Gamma\text{N}$ path in reciprocal space for bcc Fe. The solid lines are from our calculations, and the open squares are experimental points reported in Gao et al. (1993).

and we were therefore able to calculate their phonon frequencies and free energies.

Although no experimentally determined phonon-dispersion curves exist for hcp Fe, the quality of our calculations can be gauged by comparing the calculated phonon-dispersion for bcc Fe (done using fully spin polarised calculations) at ambient pressure, with the existing experimental data. Fig. 2 shows the phonon-dispersion curve for magnetic bcc Fe at ambient conditions compared with data obtained from inelastic neutron scattering experiments (see Gao et al., 1993); the calculated frequencies are in excellent agreement with the experimental values. The calculated elastic constants for bcc Fe (related to the slope of the acoustic branches of the phonon-dispersion curves) are also in a good agreement with experimentally determined values (Vočadlo et al., 1997). More recently, Mao et al. (2001) measured the phonon density of states of Fe up to 153 GPa using nuclear resonant inelastic X-ray scattering. Our calculated phonon density of states for bcc Fe at ambient pressure and at 3 GPa reported in that paper, are in outstanding agreement with experiment. The agreement with the hcp phase is also very good, but less exact than for the bcc phase, as our hcp simulations were done neglecting magnetic effects. However, nuclear resonant inelastic X-ray scattering gives a very indirect measurement of the phonon density of states, and more research is needed to establish the precision of such high pressure measurements.

The thermal pressure of hcp Fe at core conditions has been estimated to be 58 GPa (Anderson, 1995) and 50 GPa (Stixrude et al., 1997); these are in excellent agreement with our calculated thermal pressure for the hcp structure (58 GPa at 6000 K). By analysing the total pressure as a function of temperature obtained from our calculations for the potential phases of Fe, we were able to ascertain the temperature as a function of volume at two pressures ($P = 325$ GPa and $P = 360$ GPa) that span the inner-core range of pressures. From this we could determine the Gibbs free energy of these structures at those T and P . We found that, on the basis of lattice dynamic calculations over the whole P/T space investigated, the hcp phase of Fe has the lowest Gibbs free energy, and is therefore the stable form of Fe under core conditions.

Despite the fact that bcc Fe is mechanically unstable at high pressure and low temperatures (and so not amenable to lattice dynamical modelling), it has been suggested that it may become entropically stabilised at high temperatures (e.g. Matsui and Anderson, 1997). This behaviour is found in some other transition metal phases, such as Ti and Zr (see for example Liu and Bassett, 1986). We have recently performed molecular dynamic simulations of bcc Fe and have found that this structure indeed seems to become mechanically stable above ~ 1000 K at core densities. The full details of its behaviour are still to be resolved, and specifically the high P/T stability of bcc Fe relative to hcp Fe is the subject of continuing research.

6. The high P melting of Fe

Having shown how ab initio calculations are being used to establish the sub-solidus phase relations in high P Fe, we turn now to completing the description of the high P/T phase diagram of Fe, by considering its melting behaviour. An accurate knowledge of the melting properties of Fe is particularly important, as the temperature distribution in the core is relatively uncertain and a reliable estimate of the melting temperature of Fe at the pressure of the inner-core boundary (ICB) would put a much-needed constraint on core temperatures. As with the sub-solidus behaviour of Fe, there is much controversy over its high P melting behaviour (e.g. see Shen and Heinze, 1998). Static compression measurements of the melting temperature, T_m , with the

DAC have been made up to ~ 200 GPa (e.g. [Boehler, 1993](#)), but even at lower pressures results for T_m disagree by several hundred Kelvin. Shock experiments are at present the only available method to determine melting at higher pressures, but their interpretation is not simple, and there is a scatter of at least 2000 K in the reported T_m of Fe at ICB pressures (see [Nguyen and Holmes, 1999](#)).

Since both our calculations and recent experiments ([Shen et al., 1998](#)) suggest that Fe melts from the ϵ -phase in the pressure range immediately above 60 GPa, we focus here on equilibrium between hcp Fe and liquid phases. The condition for two phases to be in thermal equilibrium at a given temperature, T , and pressure, P , is that their Gibbs free energies, $G(P, T)$, are equal. To determine T_m at any pressure, we calculate G for the solid and liquid phases as a function of T and determine where they are equal. In fact, we calculate the Helmholtz free energy, $F(V, T)$, as a function of volume, V , and hence obtain the pressure through the relation $P = -(\partial F/\partial V)_T$ and G through its definition $G = F + PV$.

To obtain melting properties with useful accuracy, free energies must be calculated with high precision, because the free energy curves for liquid and solid cross at a shallow angle. It can readily be shown that to obtain T_m with a technical precision of 100 K, non-cancelling errors in G must be reduced below 10 meV. Errors in the rigid-lattice free energy due to basis-set incompleteness and Brillouin-zone sampling are readily reduced to a few meV per atom. In this study, the lattice vibrational frequencies were obtained by diagonalizing the force-constant matrix; this matrix was calculated by our ([Alfè, 1998](#)) implementation of the small-displacement method described by [Kresse et al. \(1995\)](#). The difficulty in calculating the harmonic free energy is that frequencies must be accurately converged over the whole Brillouin-zone. This requires that the free energy is fully converged with respect to the range of the force-constant matrix. To attain the necessary precision we used repeating cells containing 36 atoms, and to show that such a system gives converged energies, we performed some highly computationally demanding calculations on cells of

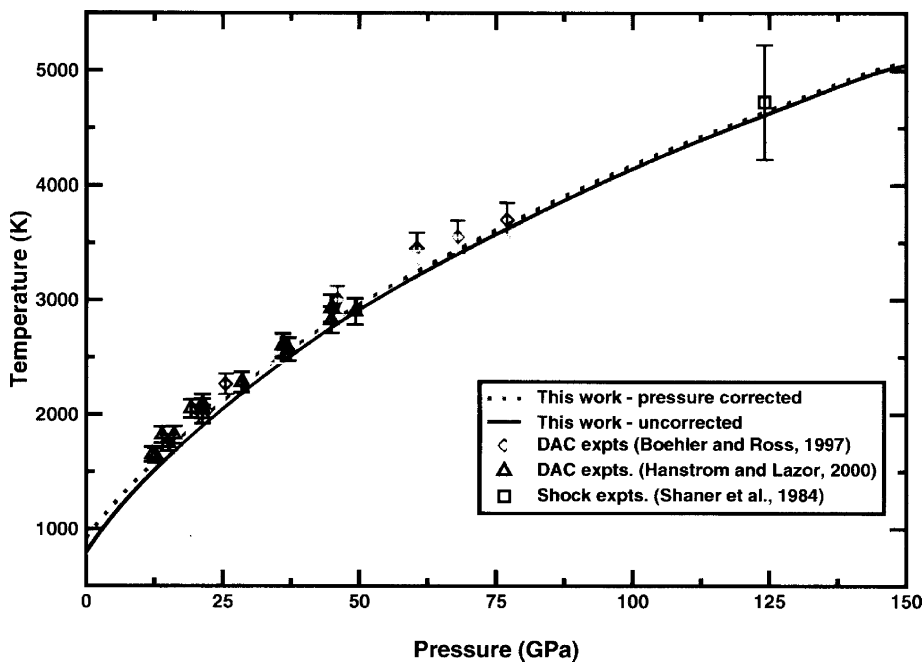


Fig. 3. Our calculated high pressure melting curve for Al (see [Vočadlo and Alfè, 2002](#)) is shown passing through a variety of recent high P experimental points.

up to 150 atoms. The anharmonic contributions to the free energy of the solid, and the free energies of the liquid were calculated by molecular dynamics, using thermodynamic integration.

To confirm that the methodology can be used accurately to calculate melting temperatures, we modelled the well studied high P melting behaviour of Al (de Wijs et al., 1998; Vočadlo and Alfè, 2002). Fig. 3 shows the excellent agreement that we obtained for this system. In 1999 we published an ab initio melting curve for Fe (Alfè et al., 1999). Since the work reported in that paper, we have improved our description of the ab initio free energy of the solid, and have revised our estimate of T_m of Fe at ICB pressures to be ~ 6250 (see Fig. 4 and Alfè et al. (2002b,d)), with an error of ± 300 K. A full analysis of the errors has been reported in Alfè et al. (2002b,d). For pressures $P < 200$ GPa (the range covered by DAC experiments) our curve lies ~ 900 K above the values of Boehler

(1993) and ~ 200 K above the more recent values of Shen et al. (1998) (who stress that their values are only a lower bound to T_m). Our curve falls significantly below the shock-based estimates for the T_m of Yoo et al. (1993), in whose experiments temperature was deduced by measuring optical emission (however, the difficulties of obtaining temperature by this method in shock experiments are well known), but accords almost exactly with the shock data value of Brown and McQueen (1986) and the new data of Nguyen and Holmes (1999). For melting at ICB pressure, we calculate $\Delta V_m/V = 1.8\%$, $\Delta S_m = 1.05 R J K^{-1} \text{ mol}^{-1}$, and so obtain a latent heat of fusion of 55 kJ mol^{-1} .

There are other ways of determining the melting temperature of a system by ab initio methods, including performing simulations that model co-existing liquid and crystal phases. The melting temperature of such a system can then be inferred by seeing which of the two phases grows during the course of a series of

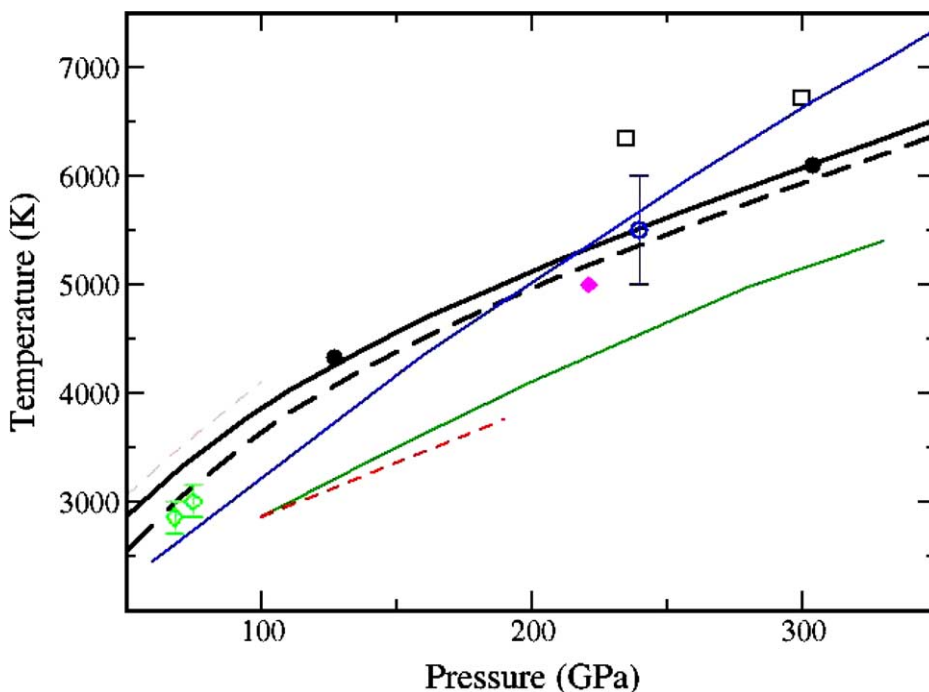


Fig. 4. Our calculated high P melting curve of Fe (plotted as a solid black line) is shown passing through the shock-wave datum (open blue circle) of Brown and McQueen (1986). Other data shown includes: our melting curve corrected for the GGA pressure error (black dashed line), Belonosko's melting curve (blue line), Belonosko's melting data corrected for potential errors (black dots), Lao et al.'s melting curve (green line), Boehler's DAC curve (green dashed line), Shen's data (green diamonds), Yoo's shock data (open squares), William's melting curve (pale green dashed line). (For interpretation of the references to colour in this figure legend, the reader is referred to the web version of this article.)

simulations at different temperatures. This approach has been used by Laio et al. (2000) and by Belonosko et al. (2000) to study the melting of Fe. In their studies they modelled Fe melting using interatomic potentials fitted to ab initio surfaces. We discovered, however, that their fitted potentials did not simultaneously describe the energy of the liquid and crystalline phases with the same precision, and so their simulations do not represent the true melting behaviour of Fe, but rather that of the fitted potential. We have recently also used the co-existence method (Alfè et al., 2002d), but with a model potential fitted to our own ab initio calculations. Initially, our raw model failed to give the same melting temperature as obtained from our ab initio free energy method, but when the results were corrected for the free energy mismatch of the model potential with respect to the ab initio energies of liquid and solid, the results for the two methods came into agreement. Thus it would seem as a general principle that there is a way to correct for the shortcomings of model potential co-existence calculations, namely one must calculate the free energy differences between the model and the ab initio system for both the liquid and solid phases. This difference in free energy between liquid and solid can then be transformed into an effective temperature correction. When this is done to Belonosko's data, there is excellent agreement with our ab initio melting curve for Fe.

As recently highlighted by Cahn (2001), there is still scope for further work on the difficult problem of the modelling of melting, but for the high P melting of Fe it appears that there may be more problems with reconciling divergent experimental data than there are in obtaining accurate predictions of T_m from ab initio studies.

7. The thermodynamic properties of hcp Fe

In the course of performing the free energy calculations outlined above, we calculated a number of other thermodynamic properties of Fe, which are of geophysical significance. In this section, we outline our calculated thermodynamic properties of hcp Fe, and in the following section, we outline the properties of liquid Fe. As the only experimental data on Fe under true core P and T comes from shock experiments, we present first the results of our ab initio studies of

hcp Fe along the Hugoniot. A full technical discussion of the calculations summarised here is presented in Alfè et al. (2001). However, we note that all the calculated thermodynamic properties were derived by initially determining the Helmholtz free energy, the volume dependence of which was used to infer the pressure and hence the Gibbs free energy. The calculated energies were fitted throughout to a third order Birch-Murnaghan equation of state or a polynomial function.

In a shock experiment, conservation of mass, momentum and energy requires that the pressure, P_H , the molar internal energy E_H , and the molar volume V_H in the compression wave are related by the Rankine–Hugoniot formula:

$$\frac{1}{2}P_H(V_0 - V_H) = E_H - E_0 \quad (10)$$

where E_0 and V_0 are the internal energy and volume in the zero-pressure state before the arrival of the wave. The quantities directly measured are the shock-wave and material velocities, which allow the values of P_H and V_H to be deduced. From a series of experiments, P_H as a function of V_H (the so-called Hugoniot) can be derived. The measurement of temperature in shock experiments has been attempted but is problematic (e.g. Yoo et al., 1993). The Hugoniot curve $P_H(V_H)$ is straightforward to compute from our results: for a given V_H , one seeks the temperature at which the Rankine–Hugoniot relation is satisfied; from this, one obtains P_H (and, if required, E_H). In experiments on Fe, V_0 and E_0 refer to the zero-pressure bcc crystal, and we obtain their values directly from GGA calculations.

Our ab initio Hugoniot is in good agreement with that measured by Brown and McQueen (1986), with discrepancies ranging from 10 GPa at $V = 7.8 \text{ \AA}^3$ to 12 GPa at $V = 8.6 \text{ \AA}^3$. These discrepancies can be regarded as giving an indication of the intrinsic accuracy of the GGA itself. Another way of looking at the accuracy to be expected of the GGA is to recalculate the Hugoniot using the experimental value of the bcc V_0 (11.8 \AA^3 , compared with the ab initio value of 11.55 \AA^3). A similar comparison with the experimental Hugoniot was given in the tight-binding total-energy work of Wasserman et al. (1996) and their agreement was as good as ours.

Our Hugoniot temperature as a function of pressure is compared with the experimental results of Yoo et al.

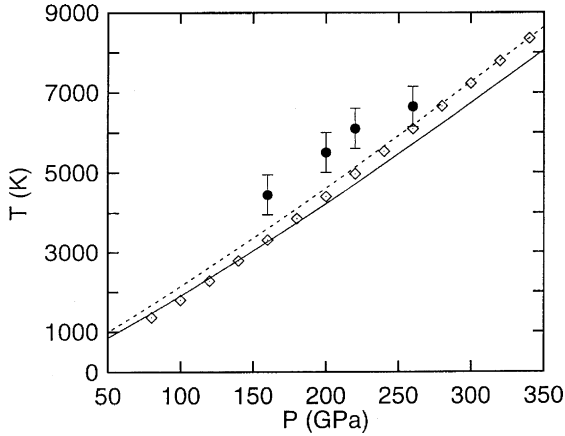


Fig. 5. Experimental and ab initio temperature as a function of pressure on the Hugoniot. The black circles are the data of Yoo et al. (1993) and the white diamonds are those of Brown and McQueen (1986). The solid curve is the ab initio data obtained when the calculated volume of bcc Fe is used in the Hugoniot-Rankine equation; the dotted curve is the same, but with the experimental equilibrium volume of bcc Fe. The comparison is meaningful only up to a pressure of ~ 250 GPa, at which point the experiments indicate melting.

(1993) in Fig. 5. We also include in the figure the estimates for Hugoniot temperature due to Brown and McQueen (1986). The latter estimates were based on the basic thermodynamic relation:

$$dT = -T \left(\frac{\gamma}{V} \right) dV + \frac{[(V_0 - V) dP + (P - P_0) dV]}{2C_v} \quad (11)$$

between infinitesimal changes of dT , dV , and dP along the Hugoniot. This relation contains the constant-volume specific heat C_v and the Grüneisen parameter γ , for which Brown and McQueen had to make assumptions. Our ab initio temperatures fall substantially below those of Yoo et al., and this supports the suggestion of Wasserman et al. (1996) that the Yoo et al. measurements overestimate the Hugoniot temperature by ~ 1000 K. On the other hand, our temperatures agree rather closely with the Brown and McQueen estimates. When we examine below their assumptions about C_v and γ , we shall see that they were reasonable, though the agreement between their temperatures and ours is also partly due to cancellation of errors between terms they use to evaluate Eq. (11).

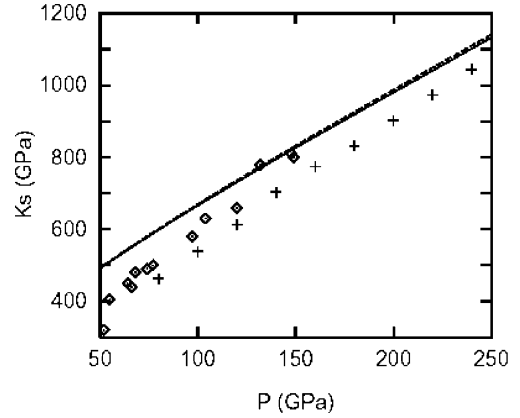


Fig. 6. Experimental and ab initio adiabatic bulk modulus (K_S) on the Hugoniot. The white diamonds are the data of Jeanloz (1979) and the crosses are those of Brown and McQueen (1986). The solid curve is the ab initio data obtained when the calculated volume of bcc Fe is used in the Hugoniot-Rankine equation; the dotted curve is the same, but with the experimental equilibrium volume of bcc Fe.

A further quantity that can be extracted from shock experiments is the bulk sound velocity v_B as a function of atomic volume on the Hugoniot, which is given by $v_B = (K_S/\rho)^{1/2}$, where $K_S \equiv -V(dP/dV)_S$ is the adiabatic bulk modulus and ρ is the mass density. Since K_S can be calculated from our ab initio pressure and entropy as functions of V and T , our calculated K_S can be directly compared with experimental values (Fig. 6). Here, there is a greater discrepancy than one would wish, with the theoretical values falling significantly above the K_S values of both Brown and McQueen (1986) and Jeanloz (1979), although we note that the two sets of experimental results disagree by an amount comparable with the discrepancy between theory and experiment.

We turn now to the more general thermodynamic properties of hcp Fe off the Hugoniot, and make some further comparisons with the predictions of Stixrude et al. (1997) and Wasserman et al. (1996). Our results are presented as a function of pressure on isotherms at $T = 2000, 4000$, and 6000 K. At each temperature, we give results only for the pressure range where, according to our calculations the hcp phase is thermodynamically stable. In comparing with the predictions of Stixrude et al. (1997) and Wasserman et al. (1996), we show the explicit numerical results from Wasserman et al. (1996) for thermodynamic quantities

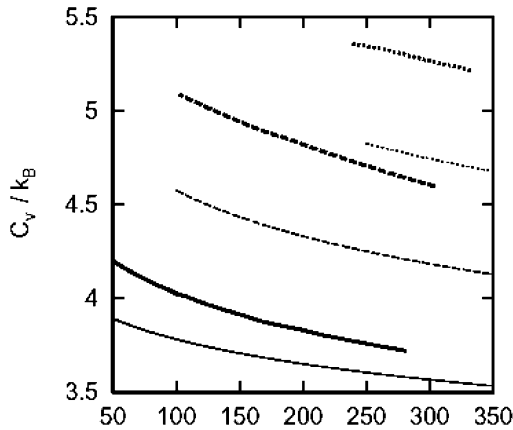


Fig. 7. Total constant-volume specific heat per atom (C_v , in units of k_B) of hcp Fe as a function of pressure on isotherms $T = 2000$ K (continuous curves), 4000 K (dashed curves), and 6000 K (dotted curves). Heavy and light curves show present results and those of Stixrude et al. (1997), respectively.

on the 2000 K isotherm. For the higher temperatures, we rely on the approximate parameterised formulas given in Stixrude et al. (1997).

The total constant-volume specific heat per atom C_v (Fig. 7) emphasises again the importance of electronic excitations. In a purely harmonic system, C_v would be equal to $3k_B$, and it is striking that C_v is considerably greater than that even at the modest temperature of 2000 K, while at 6000 K it is nearly doubled. The decrease of C_v with increasing pressure evident in Fig. 7 comes from the suppression of electronic excitations by high compression, and to a smaller extent from the suppression of anharmonicity. We note that our C_v values are significantly higher than those of Stixrude et al. (1997) and Wasserman et al. (1996); the main reason for this seems to be our inclusion of anharmonic corrections via AIMD and the T -dependence of harmonic frequencies. As stated above, Brown and McQueen (1986) made assumptions about the high P/T behaviour of C_v in order to estimate the Hugoniot temperature. Their assumptions were that the lattice contribution to C_v is equal to $3k_B$ above the Debye temperature and that the electronic contribution could be represented in the form $\beta_e(V/V_{\text{ref}})^\delta T$, where V_{ref} is a reference density, and β_e and δ are constants whose values were taken from earlier theoretical calculations. Since anharmonic and electronic contributions are negligible at low temperatures, our calculated C_v

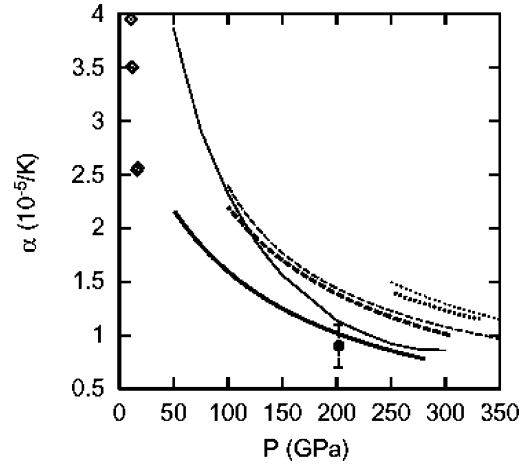


Fig. 8. The thermal expansivity (α) of hcp Fe as a function of pressure on isotherms $T = 2000$ K (continuous curves), 4000 K (dashed curves), and 6000 K (dotted curves). Heavy and light curves show present results and those of Stixrude et al. (1997), respectively. The black circle is the experimental value of Duffy and Ahrens (1993) at $T = 5200 \pm 500$ K. Diamonds are data from Boehler et al. (1990) for temperatures between 1500 and 2000 K.

agrees with the Brown and McQueen values on the low P/T part of the Hugoniot. However, our C_v rises slightly faster, mainly because of anharmonicity, and becomes $\sim 3\%$ higher than theirs at 200 GPa, the difference between the two decreasing again thereafter.

The thermal expansivity α (Fig. 8) is one of the few cases where we can compare with DAC measurements (e.g. Boehler et al., 1990). The latter show that α decreases strongly with increasing pressure and our ab initio results fully confirm this. Our results also show that α increases significantly with temperature. Both trends are also shown by the calculations of Stixrude et al. (1997) and Wasserman et al. (1996), though the latter differ from ours in showing considerably larger values of α at low pressure and temperature. The product αK_T of expansivity and isothermal bulk modulus, which is equal to $(dP/dT)_v$, is important because it is sometimes assumed to be independent of pressure and temperature over a wide range of conditions, and this constancy is used to extrapolate experimental data. Our predicted isotherms for αK_T (Fig. 9) indicate that its dependence on P is indeed weak, especially at low temperatures, but that its dependence on T certainly cannot be ignored, since it increases by at least 30% as T goes from 2000 to 6000 K at high

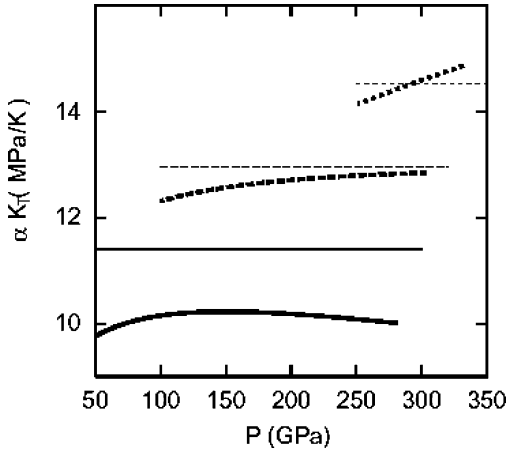


Fig. 9. The product of the expansion coefficient (α) and the isothermal bulk modulus (K_T) as a function of pressure on isotherms $T = 2000$ K (continuous curves), 4000 K (dashed curves), and 6000 K (dotted curves). Heavy and light curves show present results and those of Stixrude et al. (1997), respectively.

pressures. Wasserman et al. (1996) come to qualitatively similar conclusions, and they also find values of ~ 10 MPa K $^{-1}$ at $T = 2000$ K. However, we note that the general tendency in our results for αK_T to increase with pressure at low pressures is not found in the results of Wasserman et al. (1996) at 2000 K. In particular, they found a marked increase of αK_T with decreasing P , which does not occur in our results.

The thermodynamic Grüneisen parameter $\gamma = V(dP/dE)_v = \alpha K_T V / C_v$ plays an important role in high pressure physics, because it relates the thermal pressure and the thermal energy. Assumptions about the value of γ are frequently used in reducing shock data from the Hugoniot to an isothermal state. If one assumes that γ depends only on V , then the thermal pressure and energy are related by:

$$P_{\text{th}} V = \gamma E_{\text{th}} \quad (12)$$

the well known Mie-Grüneisen equation of state. At low temperatures, where only harmonic phonons contribute to E_{th} and P_{th} , γ should indeed be temperature independent above the Debye temperature, because $E_{\text{th}} = 3k_B T$ per atom, and $P_{\text{th}} V = -3k_B T(d \ln \omega / d \ln V) = 3k_B T \gamma_{\text{ph}}$, so that $\gamma = \gamma_{\text{ph}}$ (the phonon Grüneisen parameter) which depends only on V . But in high T Fe, the temperature independence of γ will clearly fail, because of electronic excitations

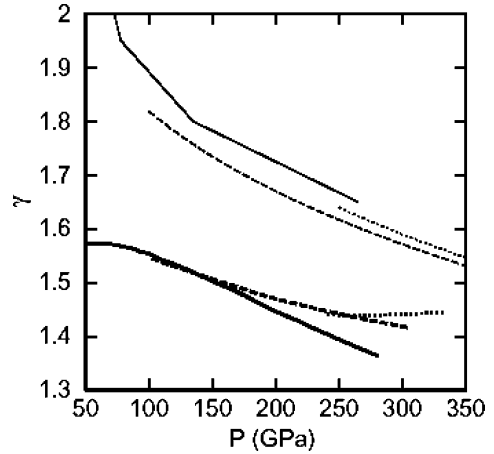


Fig. 10. The Grüneisen parameter (γ) as a function of pressure on isotherms $T = 2000$ K (continuous curves), 4000 K (dashed curves), and 6000 K (dotted curves). Heavy and light curves show present results and those of Stixrude et al. (1997), respectively.

and anharmonicity. Our results for γ (Fig. 10) indicate that it varies rather little with either pressure or temperature in the region of interest. At temperatures below ~ 4000 K, it decreases with increasing pressure, as expected from the behaviour of γ_{ph} . This is also expected from the often-used empirical rule of thumb $\gamma = (V/V_0)^q$, where V_0 is a reference volume and q is a constant exponent usually taken to be roughly unity. Since V decreases by a factor of about 0.82 as P goes from 100 to 300 GPa, this empirical relation would make γ decrease by the same factor over this range, which is roughly what we see. However, the pressure dependence of γ is very much weakened as T increases, until at 6000 K, γ is almost constant. Our results agree moderately well with those of Stixrude et al. (1997) and Wasserman et al. (1996) in giving a value $\gamma = 1.5$ at high pressures, but at low pressures there is a significant disagreement, since they find a strong increase of γ to values of over 2.0 as $P > 0$, whereas our values never exceed 1.6.

In making their estimates of the Hugoniot temperature, Brown and McQueen (1986) assumed that $(dE/dP)_v = V/\gamma$ is a constant equal to 2.85×10^{-6} m 3 mol $^{-1}$. This implies that γ is ~ 2.2 on the low P/T part of the Hugoniot, whereas our calculations give $\gamma \sim 1.5$. However, with increasing pressure, the Brown–McQueen value of γ approaches ours, being only $\sim 8\%$ higher at 200 GPa. Given the

differences between their C_v and γ values and ours, one might expect a larger disagreement between their Hugoniot temperatures and ours. However, it turns out that there is some cancellation between the differences in the various terms of Eq. (11) which brings the temperature curves into the quite close agreement that we have seen (Fig. 6).

The elastic constants of hcp Fe at 39 and 211 GPa have been measured in an experiment reported by Mao et al. (1999). Calculations of a thermal elastic constants for hcp Fe have been reported by Stixrude and Cohen (1995), Söderlind et al. (1996) and Steinle-Neumann et al. (1999). These values, together with values that we have calculated are presented in Table 1, and plotted as a function of density in Fig. 11a and b. Although there is some scatter on the reported values of c_{12} , overall the agreement between the experimental and various ab initio studies are excellent. The resulting bulk and shear moduli and the seismic velocities of hcp Fe as a function of pressure

are shown in Figs. 12 and 13, along with experimental data. The calculated values compare well with experimental data at higher pressures, but discrepancies at lower pressures are probably due to the neglect of magnetic effects in the simulations. The effect of temperature on the elastic constants of Fe have been modelled by Steinle-Neumann et al. (2001) using the PIC method. They found a significant change in the c/a ratio of the hcp structure with temperature, which causes a marked reduction in c_{33} , c_{44} and c_{66} with increasing temperature. This led them to conclude that increasing temperature reverses the sense of the single crystal longitudinal anisotropy of hcp Fe. Our calculations (Gannarelli et al., 2003) have failed thus far to reproduce the strong effect of temperature on c/a seen by Steinle-Neumann et al., and if this result is confirmed by more precise molecular dynamic simulations, then it will have important implications for the interpretation of the seismic tomography of the inner-core.

Table 1

A compilation of elastic constants (c_{ij} , in GPa), bulk (K) and shear (G) moduli (in GPa), and longitudinal (v_p) and transverse (v_s) sound velocity (in km s^{-1}) as a function of density (ρ , in g cm^{-3}) and atomic volume (in \AA^3 per atom)

V	ρ	c_{11}	c_{12}	c_{13}	c_{33}	c_{44}	c_{66}	K	G	v_p	v_s
Stixrude and Cohen											
9.19	10.09	747	301	297	802	215	223	454	224	8.64	4.71
7.25	12.79	1697	809	757	1799	421	444	1093	449	11.50	5.92
Steinle-Neumann et al.											
8.88	10.45	930	320	295	1010	260	305	521	296	9.36	5.32
7.40	12.54	1675	735	645	1835	415	470	1026	471	11.49	6.13
6.66	13.93	2320	1140	975	2545	500	590	1485	591	12.77	6.51
Mao et al.											
9.59	9.67	500	275	284	491	235	113	353	160	7.65	4.06
7.36	12.60	1533	846	835	1544	583	344	1071	442	11.48	5.92
Söderlind et al.											
9.70	9.56	638	190	218	606	178	224	348	200	8.02	4.57
7.55	12.29	1510	460	673	1450	414	525	898	448	11.03	6.04
6.17	15.03	2750	893	1470	2780	767	929	1772	789	13.70	7.24
This study											
9.17	10.12	672	189	264	796	210	242	397	227	8.32	4.74
8.67	10.70	815	252	341	926	247	282	492	263	8.87	4.96
8.07	11.49	1082	382	473	1253	309	350	675	333	9.86	5.38
7.50	12.37	1406	558	647	1588	381	424	900	407	10.80	5.74
6.97	13.31	1810	767	857	2007	466	522	1177	500	11.77	6.13
6.40	14.49	2402	1078	1185	2628	580	662	1592	630	12.95	6.59

In this table $K = ((c_{11}) + 2(c_{12}))/3$ and $G = ((c_{11}) - \langle c_{12} \rangle + 3(c_{44}))/5$, where $\langle c_{11} \rangle = (c_{11} + c_{22} + c_{33})/3$, etc. Previous calculated values are from Stixrude and Cohen (1995), Steinle-Neumann et al. (1999), Söderlind et al. (1996) and this study. The experimental data of Mao et al. (1999) is also presented.

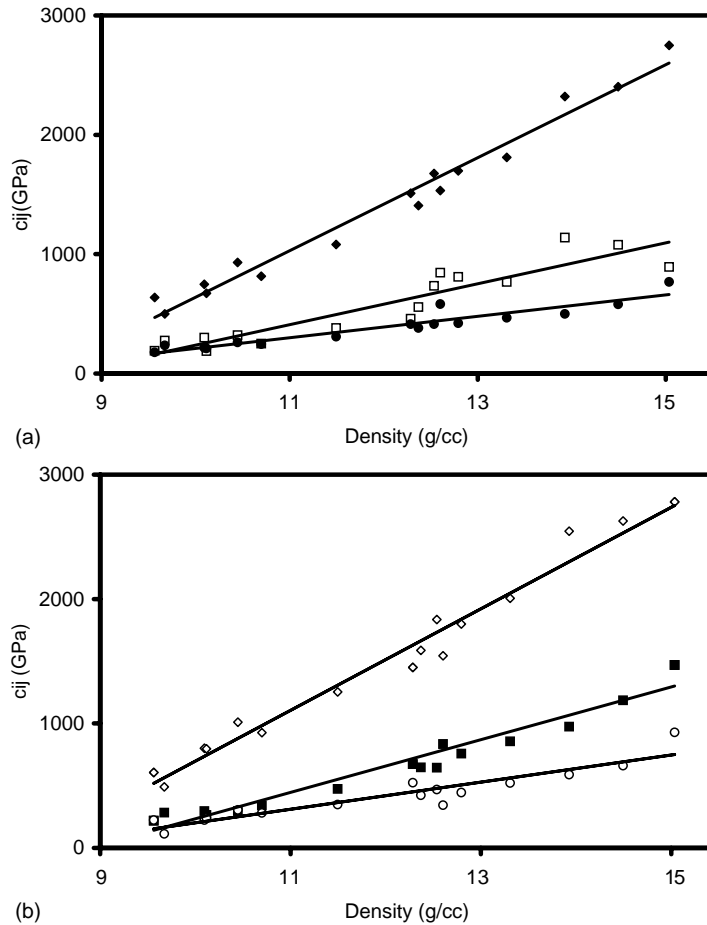


Fig. 11. Plot of elastic constants of hcp Fe given in Table 1 as a function of density: (a) c_{11} black diamonds, c_{12} white squares, c_{44} black circles, (b) c_{33} white diamonds, c_{13} black squares and c_{66} white circles.

8. Rheological and thermodynamics properties of liquid Fe

We have reported our investigation into the viscosity, diffusion and thermodynamic properties of Fe in the liquid state in de Wijs et al. (1998) and in Alfè et al. (2000). The technical details of the simulations can be found in these references. In brief, we performed PAW simulations at the 15 thermodynamic states listed in Table 2, all these simulations being done on the 67-atom system. With these simulations, we cover the temperature range 3000–8000 K and the pressure range 60–390 GPa, so that we more than cover the range of interest for the Earth's liquid core. The table

Table 2
Pressure (in GPa) calculated as a function of temperature (T) and density for liquid Fe

T (K)	ρ (kg m^{-3})				
	9540	10700	11010	12130	13300
3000	60				
4300	132 (135)				
5000	140 (145)				
6000	90	151 (155)	170 (170)	251 (240)	360 (335)
7000	161				
8000	172				

Experimental estimates are in parenthesis, from Anderson and Ahrens (1994).

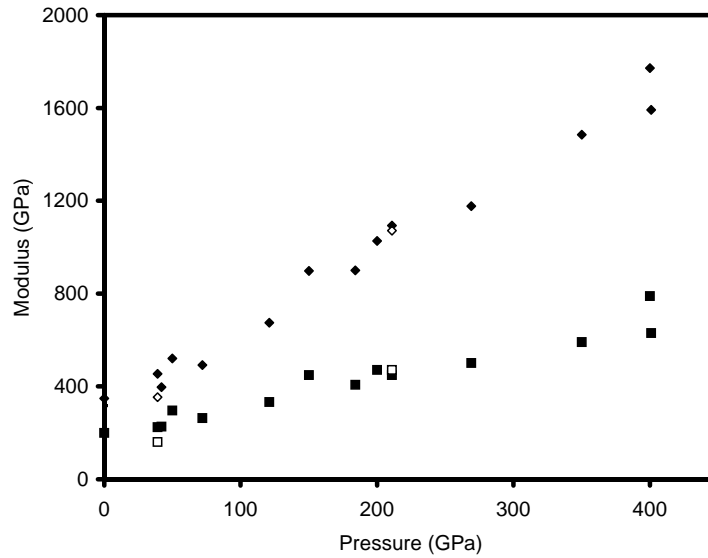


Fig. 12. Plot of bulk modulus (diamonds) and shear modulus (squares) for hcp Fe as a function of pressure, with values taken from Table 1. Black diamonds and squares represent ab initio values, while white diamonds and squares represent values obtained from experimentally determined elastic constants.

reports a comparison of the pressures calculated in the simulations with the pressures deduced by Anderson and Ahrens (1994) from a conflation of experimental data, and in Fig. 14a–f we show our calculated values

of density, thermal expansion coefficient, adiabatic and isothermal bulk moduli, heat capacity (C_v), Grüneisen parameter, and bulk sound velocity respectively. These values are in close accord with the estimates

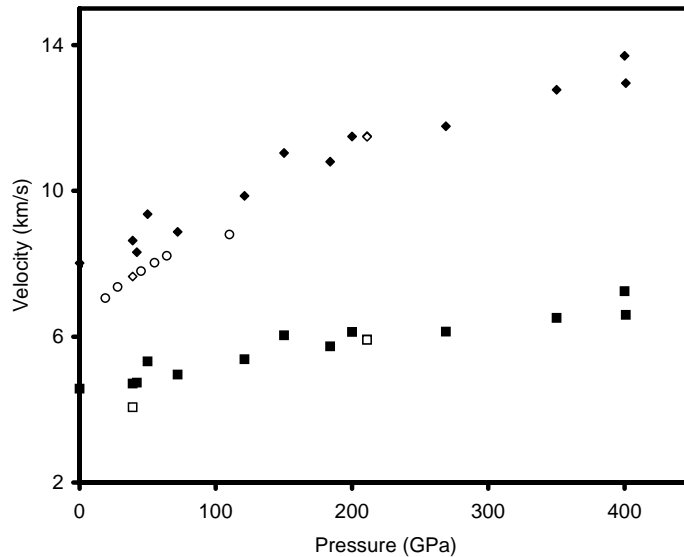


Fig. 13. Plot of aggregate v_p (diamonds) and v_s (squares) wave velocity for hcp Fe as a function of pressure, with values taken from Table 1. Black diamonds and squares represent ab initio values, while white diamonds and squares represent values obtained from experimentally determined elastic constants. White circles are the experimental data of Fiquet et al. (2001).

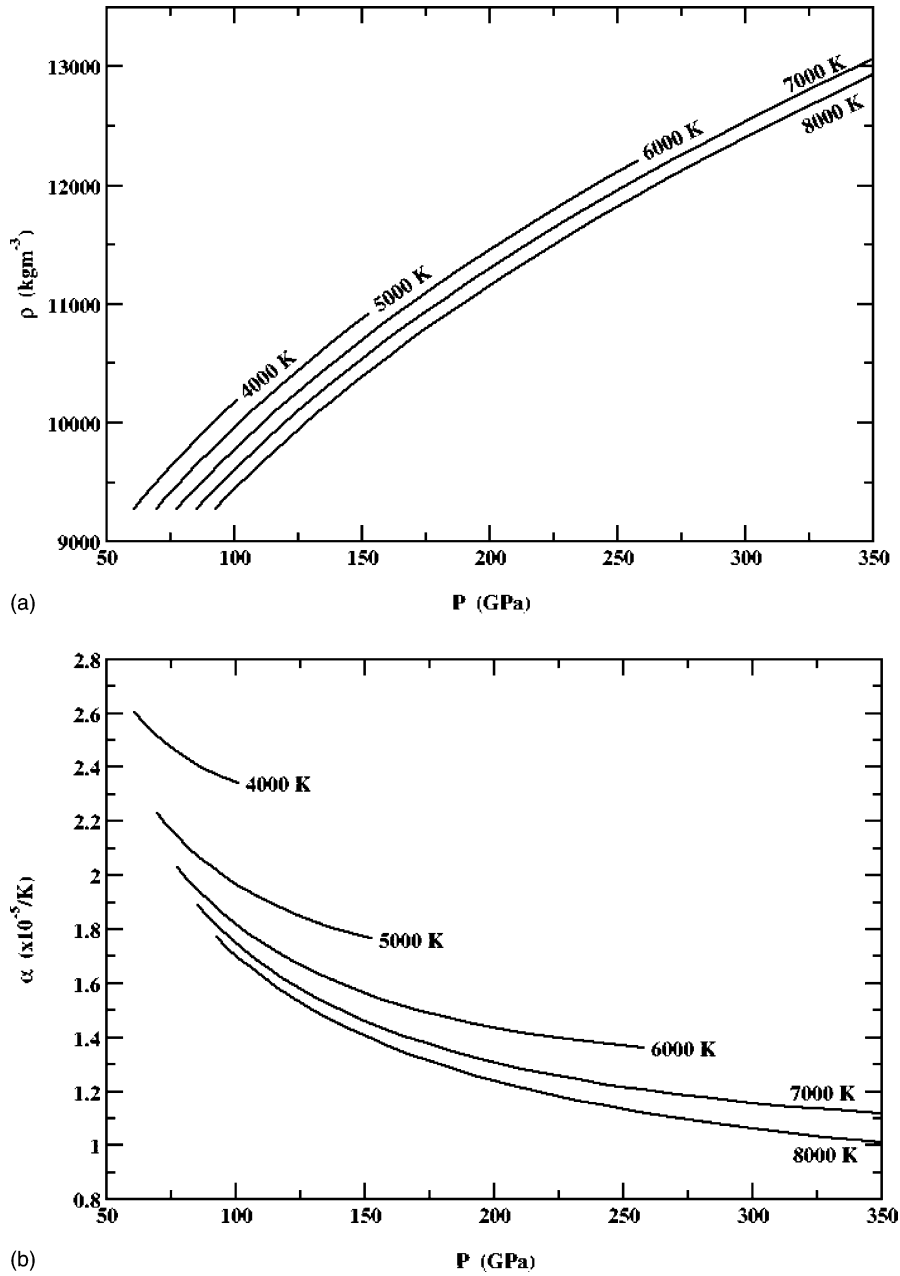


Fig. 14. Panel showing the calculated values of (a) density, (b) thermal expansion coefficient, (c) adiabatic (dashed lines) and isothermal bulk (solid lines) moduli, (d) heat capacity (C_V), (e) Grüneisen parameter, and (f) bulk sound velocity for liquid Fe, all as a function of P at temperatures between 4000 and 8000 K.

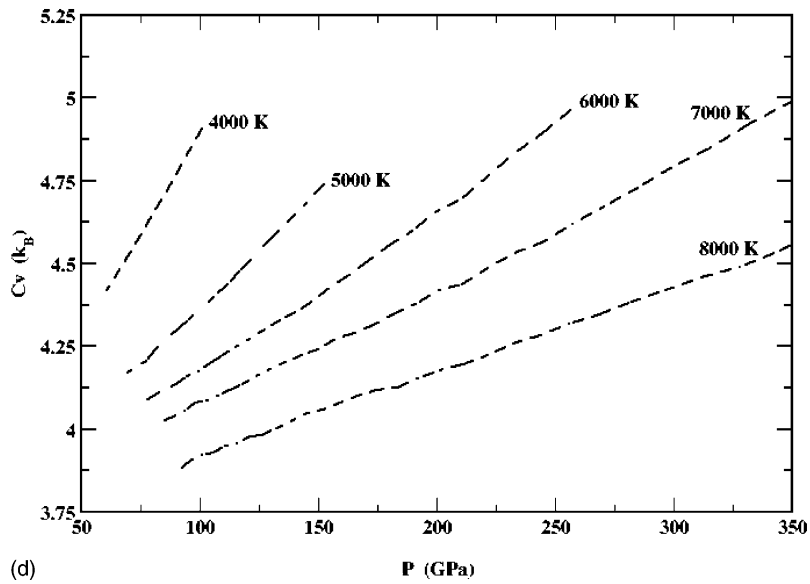
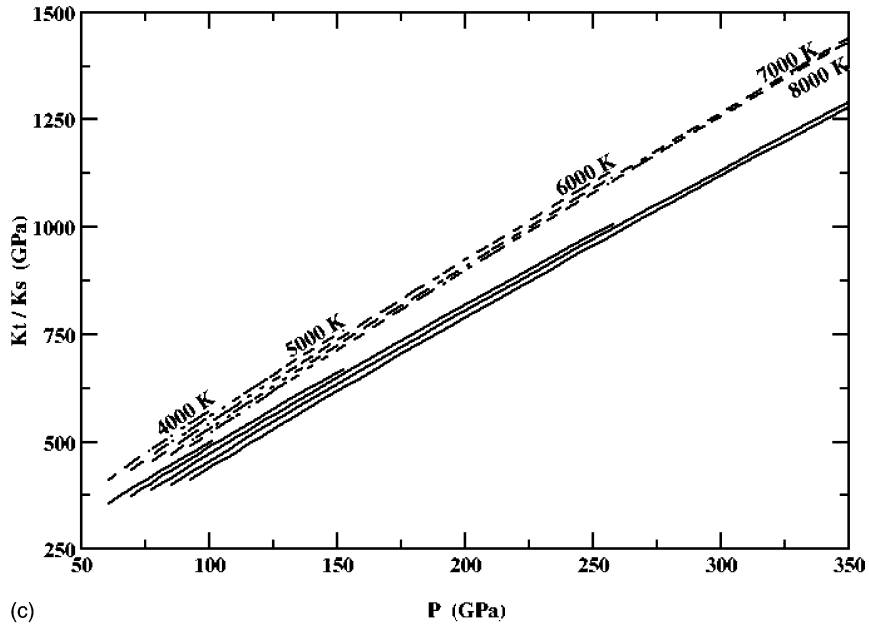


Fig. 14. (Continued).

available in Anderson and Ahrens (1994), indeed, our first principles pressures reproduce the experimental density values to within 2–3% at low densities, but they are systematically too high by $\sim 7\%$ at high densities. It is not clear yet whether the high-density discrepancies indicate a real deficiency in the ab initio

calculations rather than problems in the interpretation of the experimental data.

It is commonly found that increasing temperature significantly reduces the sound velocity in a liquid. So for iron at atmospheric pressure, dv_P/dT has been estimated by Anderson and Ahrens (1994) to

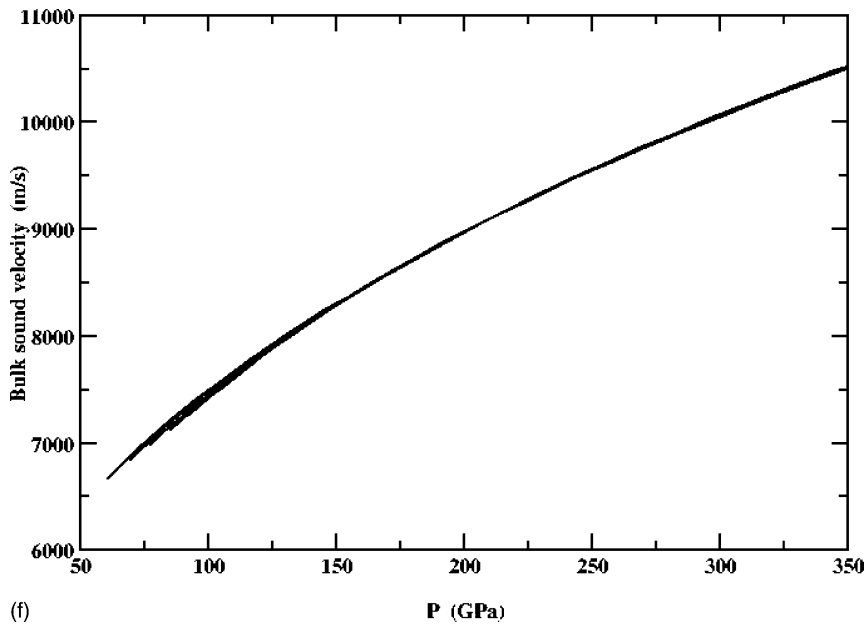
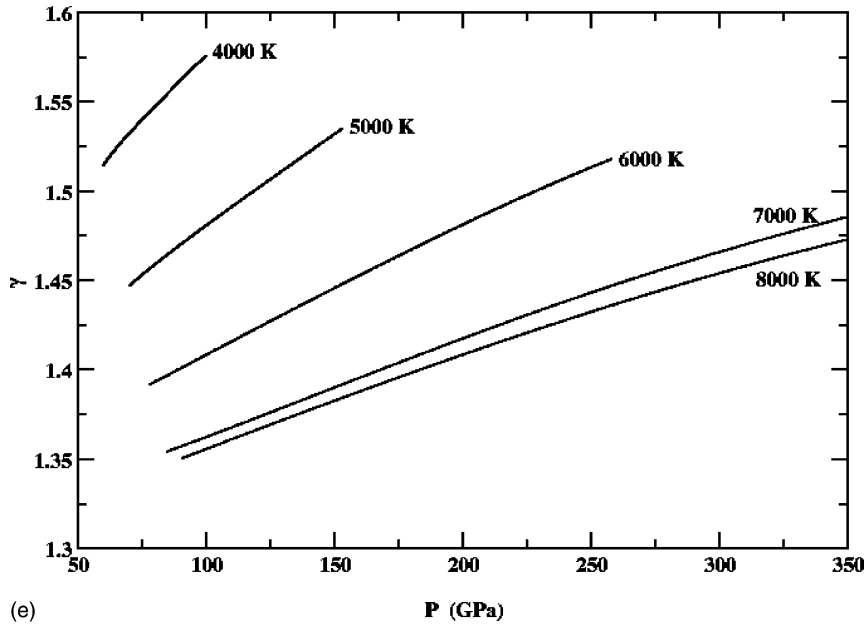


Fig. 14. (Continued).

be $\sim -0.54 \pm 0.21 \text{ ms}^{-1} \text{ K}^{-1}$. These authors subsequently reviewed the available high P data for liquid iron, and concluded that “the pure Fe isentropes are nearly indistinguishable from one another in sound

velocity”, but they did not directly calculate higher pressure values of dv_P/dT . However, the high P behaviour of dv_P/dT is important, as pointed out by Gubbins et al. (2003), as it has a direct relationship

with the variation of the Grüneisen parameter along the core adiabat, thus:

$$\left(\frac{\partial\gamma}{\partial P}\right)_S = -\left(\frac{\gamma}{K_S}\right) \left[2 + \gamma - \left(\frac{\partial K_S}{\partial P}\right)_S - \left(\frac{1}{\alpha v_P^2}\right) \left(\frac{\partial v_P^2}{\partial T}\right)_P \right] \quad (13)$$

which in turn affects the adiabatic temperature gradient in the outer core, and hence the effectiveness of the geodynamo.

In the absence of any firmer data at the time, Gubbins and Masters (1979) took $(\partial v_P^2/\partial T)_P$ to be

$-2000 \text{ m}^2 \text{ s}^{-2} \text{ K}^{-1}$ (c.f. the ambient pressure value obtained from Anderson and Ahrens (1994) of about $-4000 \text{ m}^2 \text{ s}^{-2} \text{ K}^{-1}$) when they developed their model of the core and the geodynamo. However, it is now possible to determine higher order derivatives such as $(\partial\gamma/\partial P)_S$ and $(\partial v_P^2/\partial T)_P$ from our ab initio calculations. The robustness of the derivation of these higher terms is shown in Fig. 15a, which shows $(\partial\gamma/\partial P)_S$ as obtained from numerical differentiation of the variation of our calculated Grüneisen parameter along the adiabat (Fig. 15b), and that obtained by evaluating Eq. (13), using the values calculated for $(\partial v_P^2/\partial T)_P$ shown in Fig. 15c. It is important to note that these high pressure values $(\partial v_P^2/\partial T)_P$ are significantly

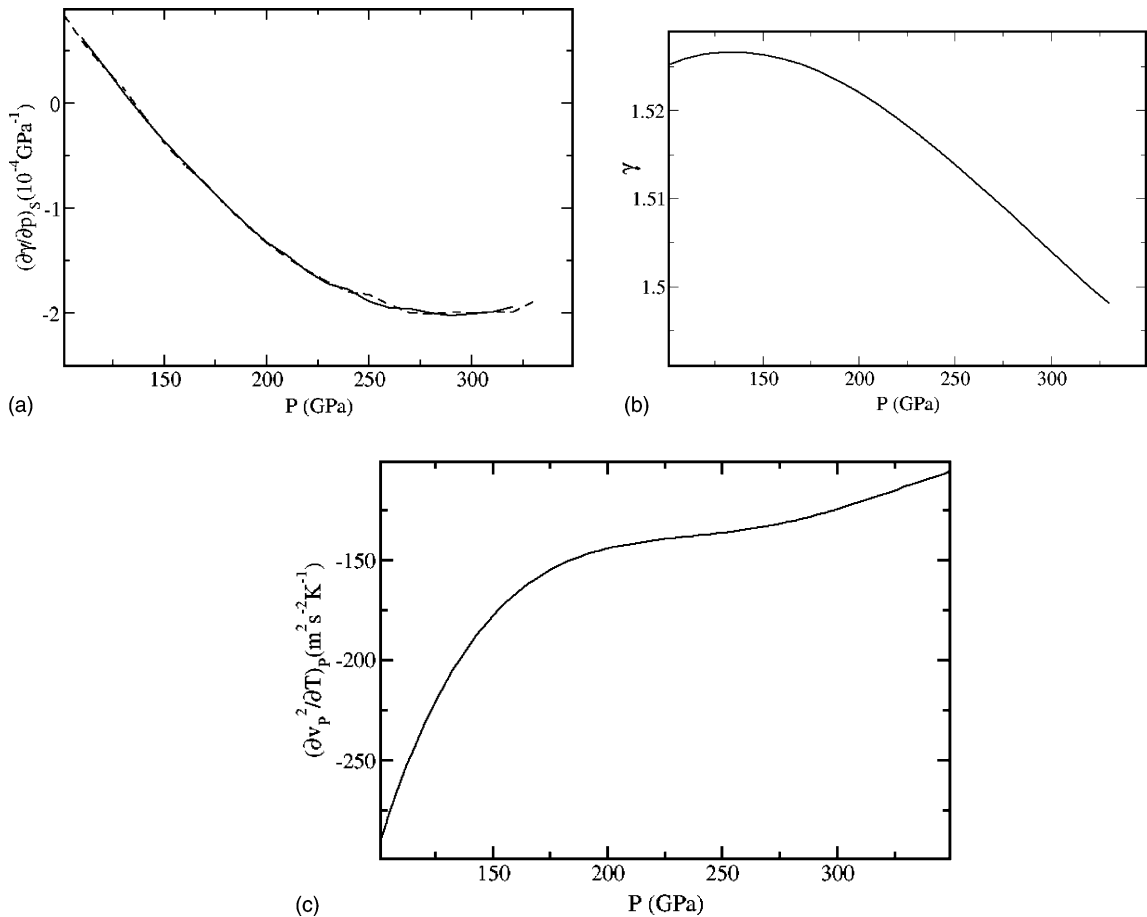


Fig. 15. (a) A plot of $(\partial\gamma/\partial P)_S$ (in GPa^{-1}) against P (in GPa) showing curves obtained by differentiation of the curves shown in 15b and by evaluation of Eq. (13). (b) The ab initio calculated variation of the Grüneisen parameter of liquid Fe along the core adiabat. (c) The calculated variation of $(\partial v_P^2/\partial T)_P$ (in $\text{m}^2 \text{ s}^{-2} \text{ K}^{-1}$) of liquid iron as a function of P (in GPa).

Table 3

The diffusion coefficient (D) and the viscosity (η) from our ab initio simulations of liquid Fe at a range of temperatures and densities

T (K)	ρ (kg m^{-3})				
	9540	10700	11010	12130	13300
D ($10^{-9} \text{ m}^2 \text{ s}^{-1}$)					
3000	4.0 ± 0.4				
4300	5.2 ± 0.2				
5000	7.0 ± 0.7				
6000	14 ± 1.4	10 ± 1	9 ± 0.9	6 ± 0.6	5 ± 0.5
7000		13 ± 1.3	11 ± 1.1	9 ± 0.9	6 ± 0.6
η (mPa s)					
3000	6 ± 3				
4300	8.5 ± 1				
5000	6 ± 3				
6000	2.5 ± 2	5 ± 2	7 ± 3	8 ± 3	15 ± 5
7000		4.5 ± 2	4 ± 2	8 ± 3	10 ± 3

The error estimates come from statistical uncertainty due to the short duration of the simulations.

smaller than the ambient pressure value, and that any model of core behaviour should use these more appropriate values. Although not explicitly presented in Anderson and Ahrens (1994), it is possible to estimate a value for $(\partial v_p^2 / \partial T)_P$ from their Fig. 10, which yields a value of $\sim -140 \text{ m}^2 \text{ s}^{-2} \text{ K}^{-1}$ at the ICB, in excellent agreement with our ab initio calculation.

In Table 3, we report values for the self diffusion of Fe in liquid Fe, and the viscosity of liquid Fe for the same range of P and T conditions reported above. Since most of the simulations reported in Table 3 are rather short (typically no more than 4 ps) the statistical accuracy on D and η is not great (the error estimates also reported in Table 3). These ab initio simulations demonstrate that under Earth's core conditions liquid Fe is a typical simple liquid. In common with other simple liquids, like liquid Ar and Al, it has a close-packed structure, the coordination number in the present case being ~ 13 . In fact, there appears to be a truly remarkable simplicity in the variation of the liquid properties of Fe with thermodynamic state. To show the relative independence of the radial distribution function (rdf) with temperature, we report in Fig. 16 the rdf, $g(r)$, for the five temperatures 4300, 5000, 6000, 7000, and 8000 K at the same density $\rho = 10,700 \text{ kg m}^{-3}$. The effect of varying temperature is clearly not dramatic, and consists of the expected weakening and broadening of the structure

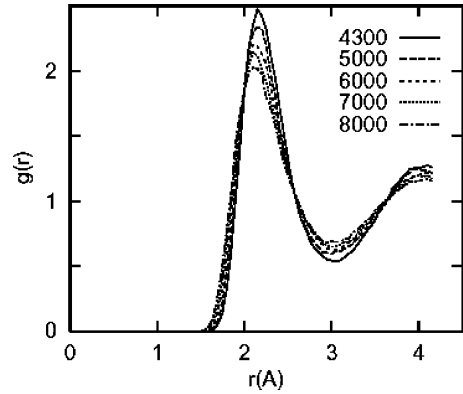


Fig. 16. The variation of the radial distribution function ($g(r)$) of liquid Fe with temperature from ab initio simulations at the fixed density of $\rho = 10.7 \text{ g cm}^{-3}$. Results are shown for the five temperatures $T = 4300, 5000, 6000, 7000$ and 8000 K .

with increasing T . For the entire pressure-temperature domain of interest for the Earth's outer core, the diffusion coefficient, D , and viscosity, η , are comparable with those of typical simple liquids, D being $\sim 5 \times 10^{-9} \text{ m}^2 \text{ s}^{-1}$ and η being in the range 8–15 mPa s, depending on the detailed thermodynamic state. Similar estimates for viscosity of liquid Fe are presented by Stixrude et al. (1998), based on calculations using the tight-binding approximation.

Since the Earth's outer core is in a state of convection, the temperature and density will lie on adiabats. It is straightforward to show that the variation of D and η along adiabats will be rather weak. For example, if we take the data for high pressure liquid iron compiled by Anderson and Ahrens (1994) then the adiabat for $T = 6000 \text{ K}$ at the inner-core boundary pressure 330 GPa has $T = 4300 \text{ K}$ at the core mantle boundary (CMB) pressure of 135 GPa. Taking the densities at these two points from the same source, we find the liquid structure virtually unchanged, apart from a trivial length scaling. For all practical purposes, then, it can be assumed that variation of thermodynamic conditions across the range found in the core has almost no effect on the liquid structure. For the same reasons, the diffusion coefficient D and viscosity also show little variation, so that the diffusion coefficient D is $5 \pm 0.5 \times 10^{-9} \text{ m}^2 \text{ s}^{-1}$ without significant variation as one goes from ICB to CMB pressures along the adiabat, and in parallel η goes from 15 ± 5 to 8.5 ± 1 mPa s. These calculations finally resolve the issue of the viscosity

of the outer core, which historically was considered to be uncertain to within 13 orders of magnitude!

9. Conclusion

The past decade has seen a major advance in the application of ab initio methods in the solution of high pressure and temperature geophysical problems, thanks to the rapid developments in high performance computing. In all of our studies of solid and liquid Fe summarised above, we have made strenuous efforts to demonstrate the robustness and reliability of our calculations. We have shown that our results are completely robust with respect to all the main technical factors: size of simulated system, k -point sampling, and choice of ab initio method. At present, ab initio dynamical simulations of the type presented here are only practicable with the PAW or pseudopotential techniques. However, our comparisons leave little doubt that if such simulations were feasible with other DFT techniques, such as FLAPW, virtually identical results would be obtained. As a result, we are confident that we are now in a position to calculate from first principles the free energies of solid and liquid phases, and hence to determine both the phase relations and the physical properties of planetary forming minerals.

In the future, we look forward to the advent of routinely available ‘terascale’ computing. This will open new possibilities for geophysical modelling. Thus, we will be able to model more complex and larger systems, to investigate for example solid state rheological problems, or physical properties such as thermal and electrical conductivity. However, we recognise that the DFT methods we currently use are still approximate, and fail for example to describe the band structure of important phases such as FeO. In the future we intend to use terascale facilities to implement more demanding but more accurate techniques, such as those based on quantum Monte Carlo methods.

Acknowledgements

We would like to thank Lars Stixrude for his very helpful comments on an early version of our manuscript. DA and LV are supported by Royal Society University Research Fellowships. MJG thanks

GEC and Daresbury Laboratory for their support. This work was supported by NERC grants GR3/12083 and GR9/03550. The calculations were run on the Cray T3D and Cray T3E machines at Edinburgh and the Manchester CSAR Centre and on the Origin 2000 machine at the UCL HiPerSPACE Centre.

References

- Alfè, D., 1998. Program available from <http://www.chianti.geol.ucl.ac.uk/~dario/phon.tar.z>.
- Alfè, D., 1999. Ab initio molecular dynamics, a simple algorithm for charge extrapolation. *Comput. Phys. Commun.* 118, 31–33.
- Alfè, D., Gillan, M.J., Price, G.D., 1999. The melting curve of iron at the pressures of the Earth’s core from ab initio calculations. *Nature* 401, 462–464.
- Alfè, D., Kresse, G., Gillan, M.J., 2000. Structure and dynamics of liquid iron under Earth’s core conditions. *Phys. Rev.* 61, 132–142.
- Alfè, D., Price, G.D., Gillan, M.J., 2001. Thermodynamics of hexagonal-close-packed iron under Earth’s core conditions. *Phys. Rev.* B64, 045123.
- Alfè, D., Gillan, M.J., Price, G.D., 2002a. Composition and temperature of the Earth’s core constrained by combining ab initio calculations and seismic data. *Earth Planet. Sci. Lett.* 195, 91–98.
- Alfè, D., Price, G.D., Gillan, M.J., 2002b. Iron under Earth’s core conditions: liquid-state thermodynamics and high-pressure melting curve from ab initio calculations. *Phys. Rev.* B65 (165118), 1–11.
- Alfè, D., Gillan, M.J., Price, G.D., 2002c. Ab initio chemical potential of solid and liquid solutions and chemistry of the Earth’s core. *J. Chem. Phys.* 116, 7127–7136.
- Alfè, D., Gillan, M.J., Price, G.D., 2002d. Complementary approaches to the ab initio calculation of melting properties. *J. Chem. Phys.* 116, 6170–6177.
- Allègre, C.J., Poirier, J.P., Humler, E., Hofmann, A.W., 1995. The chemical composition of the Earth. *Phys. Earth Planet. Interiors.* 134, 515–526.
- Allen, M.P., Tildesley, D.J., 1987. *Computer Simulation of Liquids*. Oxford University Press, Oxford, UK.
- Anderson, O.L., 1995. *Equations of State of Solids for Geophysics and Ceramic Science*. Oxford University Press, Oxford, UK.
- Anderson, W.W., Ahrens, T.J., 1994. An equation of state for liquid iron and implication for the Earth’s core. *J. Geophys. Res.* 99, 4273–4284.
- Andraut, D., Fiquet, G., Kunz, M., Visocekas, F., Häusermann, D., 1997. The orthorhombic structure of iron: an in situ study at high temperature and high pressure. *Science* 278, 831–834.
- Ball, R.D., 1989. Anharmonic lattice dynamics. In: Stoneham, A.M. (Ed.), *Anharmonic Lattice Dynamics in Ionic Solids at High Temperatures*. World Scientific, Singapore.
- Belonosko, A.B., Ahuja, R., Johansson, B., 2000. Quasi-ab initio molecular dynamic study of Fe melting. *Phys. Rev. Lett.* 84, 3638–3641.

- Birch, F., 1952. Elasticity and the constitution of the Earth's interior. *J. Geophys. Res.* 57, 227–286.
- Boehler, R., 1993. Temperature in the Earth's core from the melting point measurements of iron at high static pressures. *Nature* 363, 534–536.
- Boehler, R., 2000. High-pressure experiments and the phase diagram of lower mantle and core materials. *Rev. Geophys.* 38, 221–245.
- Boehler, R., von Bagen, N., Chopelas, A., 1990. Melting, thermal expansion and phase transitions of iron at high pressure. *J. Geophys. Res.* 95, 21731–21736.
- Born, M., Huang, K., 1954. *Dynamical Theory of Crystal Lattices*. Oxford University Press, Oxford, UK.
- Brown, J.M., 2001. The equation of state of iron to 450 GPa: another high pressure solid 18 phase? *Geophys. Res. Lett.* 28, 4339–4342.
- Brown, J.M., McQueen, R.G., 1986. Phase transitions, Grüneisen parameter and elasticity for shocked iron between 77 GPa and 400 GPa. *J. Geophys. Res.* 91, 7485–7494.
- Cahn, R.W., 2001. Melting from within. *Nature* 413, 582–583.
- Car, R., Parrinello, M., 1985. Unified approach for molecular dynamics and density functional theory. *Phys. Rev. Lett.* 55, 2471–2474.
- Cohen, M., Heine, V., 1970. The fitting of pseudopotentials to experimental data and their subsequent application. In: Ehrenreich, H., Seitz, F., Turnbull, D. (Eds.), *Solid State Physics*, vol. 24, pp. 37–248.
- de Wijs, G.A., Kresse, G., Gillan, M.J., 1998. First order phase transitions by first principles free energy calculations: the melting of Al. *Phys. Rev. B* 57, 8233–8234.
- Gannarelli, C.M.S., Alfè, D., Gillan, M.J., 2003. The particle-in-cell model for ab initio thermodynamics: implications for the elastic anisotropy of the Earth's inner core. *Phys. Earth Planet. Interiors*, submitted for publication.
- Gao, F., Johnston, R.L., Murrell, J.N., 1993. Empirical many-body potential energy functions for iron. *J. Phys. Chem.* 97, 12073–12082.
- Gillan, M.J., 1997. The virtual matter laboratory. *Contemp. Phys.* 38, 115–130.
- Heine, V., 1970. The pseudopotential concept. In: Ehrenreich, H., Seitz, F., Turnbull, D. (Eds.), *Solid State Physics*, vol. 24, pp. 1–36.
- Gubbins, D., Masters, G., 1979. Driving mechanisms for the Earth's dynamo. *Adv. Geophys.* 21, 1–50.
- Gubbins, D., Alfè, D., Masters, G., Price, G.D., Gillan, M.J., 2003. Can the Earth's dynamo run on heat alone? *Geophys. J. Int.*, in press.
- Heine, V., Weaire, D., 1970. Pseudopotential theory of cohesion and structure. In: Ehrenreich, H., Seitz, F., Turnbull, D. (Eds.), *Solid State Physics*, vol. 24, pp. 249–463.
- Hohenberg, P., Kohn, W., 1964. Inhomogeneous electron gas. *Phys. Rev. B* 136, 864–871.
- Kohn, W., Sham, L.J., 1965. Self consistent equations including exchange and correlation effects. *Phys. Rev. A* 140, 1133–1138.
- Jeanloz, R., 1979. Properties of iron at high pressures and the state of the core. *J. Geophys. Res.* 84, 6059–6069.
- Kresse, G., Furthmüller, J., 1996. Efficient iterative schemes for ab-initio total-energy calculations using a plane-wave basis set. *Phys. Rev. B* 54, 11169–11186.
- Kresse, G., Joubert, D., 1999. From ultra soft pseudopotentials to the projector augmented-wave method. *Phys. Rev. B* 59, 1758–1775.
- Kresse, G., Furthmüller, J., Hafner, J., 1995. Ab-initio force-constant approach to phonon dispersion relations of diamond and graphite. *Europhys. Lett.* 32, 729–734.
- Laio, A., Bernard, S., Chiarotti, G.L., Scandolo, S., Tosatti, E., 2000. Physics of iron at Earth's core conditions. *Science* 287, 1027–1030.
- Liu, L., Bassett, W.A., 1986. *Elements, Oxides, Silicates: High-Pressure Phases with Implications for the Earth's Interior*. OUP, New York.
- Mao, H.K., Shu, J., Shen, G., Hemley, R.J., Li, B., Sing, A.K., 1999. Elasticity and rheology of iron above 220 GPa and the nature of the Earth's inner core. *Nature* 399, 280.
- Mao, H.K., Xu, J., Struzhkin, V.V., Shu, J., Hemley, R.J., Sturhahn, W., Hu, M.Y., Alp, E.E., Vočadlo, L., Alfè, D., Price, G.D., Gillan, M.J., Schwöberer-Bohning, M., Hausermann, D., Eng, P., Shen, G., Giefers, H., Lubbers, R., Wortmann, G., 2001. Phonon density of states of iron up to 153 gigapascals. *Science* 292, 914–916.
- Matsui, M., Anderson, O.L., 1997. The case for a body-centered cubic phase for iron at inner core conditions. *Phys. Earth Planet. Interiors* 103, 55–62.
- Matsui, M., Price, G.D., Patel, A., 1994. Comparison between the lattice dynamics and molecular dynamics methods: calculation results for MgSiO₃ perovskite. *Geophys. Res. Lett.* 21, 1659–1662.
- McDonough, W.F., Sun, S.-S., 1995. The composition of the Earth. *Chem. Geol.* 120, 223–253.
- Mukherjee, S., Cohen, R.E., 2002. Tight-binding based non-collinear spin model and magnetic correlations in iron. *J. Computer-Aided Mater.* 8, 107–115.
- Nguyen, J.H., Holmes, N.C., 1999. Iron sound velocities in shock wave experiments. *Shock Compress. Condens. Matter CP505*, 81–84.
- Parker, S.C., Price, G.D., 1989. Computer modelling of phase transitions in minerals. *Adv. Solid State Chem.* 1, 295–327.
- Parrinello, M., Rahman, A., 1980. Crystal structure and pair potentials: a molecular dynamics study. *Phys. Rev. Lett.* 45, 1196–1199.
- Poirier, J.P., 1994a. Light elements in the Earth's outer core: a critical review. *Phys. Earth Planet. Inter.* 85, 319–337.
- Poirier, J.P., 1994b. Physical-properties of the Earth's core. *C.R. Acad. Sci. II* 318, 341–350.
- Pulay, P., 1980. Convergence acceleration of iterative sequences. The case of SCF iteration. *Chem. Phys. Lett.* 73, 393.
- Saxena, S.K., Dubrovinsky, L.S., Häggkvist, P., 1996. X-ray evidence for the new phase of β -iron at high temperature and high pressure. *Geophys. Res. Lett.* 23, 2441–2444.
- Shen, G.Y., Heinze, D.L., 1998. High Pressure melting of deep mantle and core materials. In: Hemley, R.J. (Ed.), *Ultra-high-Pressure Mineralogy. Reviews in Mineralogy*, vol. 37, pp. 369–398.

- Shen, G.Y., Mao, H.K., Hemley, R.J., Duffy, T.S., Rivers, M.L., 1998. Melting and crystal structure of iron at high pressures and temperatures. *Geophys. Res. Lett.* 25, 373.
- Söderlind, P., Moriarty, J.A., Wills, J.M., 1996. First-principles theory of iron up to earth-core pressures: structural, vibrational and elastic properties. *Phys. Rev.* B53, 14063–14072.
- Steinle-Neumann, G., Stixrude, L., Cohen, R.E., 1999. First-principles elastic constants for the hcp transition metals Fe, Co, and Re at high pressure. *Phys. Rev.* B60, 791–799.
- Steinle-Neumann, G., Stixrude, L., Cohen, R.E., Gülseren, O., 2001. Elasticity of iron at the temperature of the Earth's inner core. *Nature* 413, 57–60.
- Stixrude, L., Brown, J.M., 1998. The Earth's core. In: Hemley, R.J. (Ed.), *Ultrahigh-Pressure Mineralogy*. *Reviews in Mineralogy*, vol. 37, pp. 261–283.
- Stixrude, L., Cohen, R.E., 1995. Constraints on the crystalline structure of the inner core—mechanical instability of bcc iron at high-pressure. *Geophys. Res. Lett.* 22, 125–128.
- Stixrude, L., Wasserman, E., Cohen, R.E., 1997. Composition and temperature of the Earth's inner core. *J. Geophys. Res.* 102, 24729–24739.
- Stixrude, L., Cohen, R.E., Hemley, R.J., 1998. Theory of minerals at high pressure. In: Hemley, R.J. (Ed.), *Ultrahigh-Pressure Mineralogy*. *Reviews in Mineralogy*, vol. 37, pp. 639–671.
- Vanderbilt, D., 1990. Soft self-consistent pseudopotentials in a generalized eigenvalue formalism. *Phys. Rev.* B41, 7892–7895.
- Vočadlo, L., Alfè, D., 2002. The ab initio melting curve of aluminum. *Phys. Rev.* B65 (214105), 1–12.
- Vočadlo, L., deWijns, G.A., Kresse, G., Gillan, M.J., Price, G.D., 1997. First principles calculations on crystalline and liquid iron at Earth's core conditions. *Faraday Dis.* 106, 205–217.
- Vočadlo, L., Brodholt, J., Alfè, D., Price, G.D., Gillan, M.J., 1999. The structure of iron under the conditions of the Earth's inner core. *Geophys. Res. Lett.* 26, 1231–1234.
- Wang, Y., Perdew, J.P., 1991. Correlation hole of the spin-polarized electron-gas, with exact small-wave-vector and high-density scaling. *Phys. Rev.* B44, 13298–13307.
- Wasserman, E., Stixrude, L., Cohen, R.E., 1996. Thermal properties of iron at high pressures and temperatures. *Phys. Rev.* B53, 8296–8309.
- Yoo, C.S., Holmes, N.C., Ross, M., Webb, D.J., Pike, C., 1993. Shock temperatures and melting of iron at Earth core conditions. *Phys. Rev. Lett.* 70, 3931–3934.